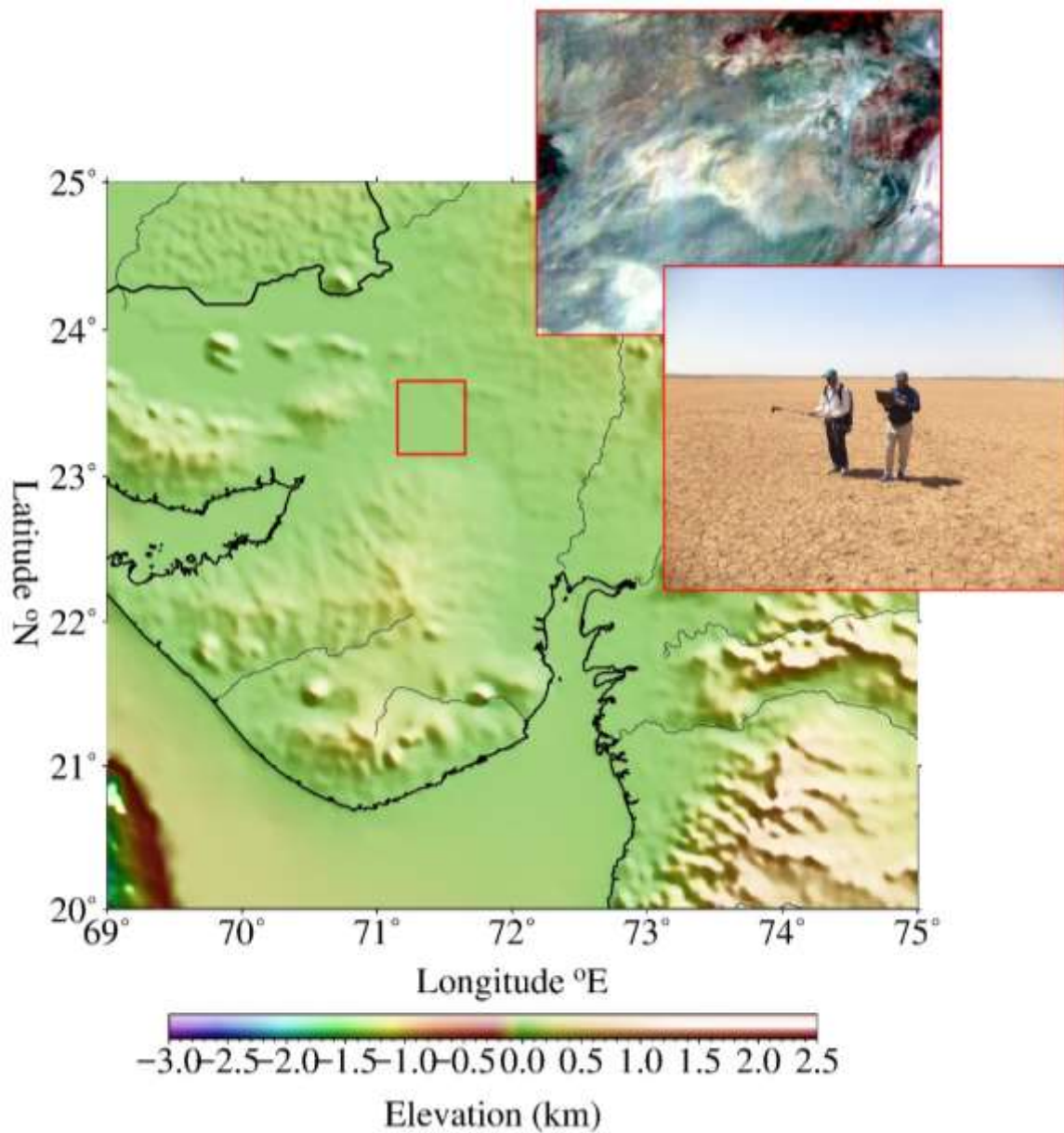


The vicarious calibration of HySIS over desert site



K N Babu, Nandkishor, Anuj and A K Mathur

Calibration-Validation Division (CVD)
Earth, Ocean, Atmosphere, Planetary Sciences & Applications Area (EP SA)
Space Applications Centre (ISRO)
Ahmadabad – 380 015

Document control sheet

1. Report No.	SAC/EPESA/CVD/CAL-VAL/2019/001
2. Publication Date	April, 2019
3. Title	The vicarious calibration of HySIS over desert site
4. Type of Report	Scientific
5. Number of pages	23
6. Number of references	29
7. Authors	K. N. Babu, Nandkishor, Anuj and A. K. Mathur
8. Originating unit	CVD-EPESA
9. Abstract	<p>The absolute radiometric calibration of a satellite sensor is the critical factor that ensures the usefulness of the acquired data for quantitative applications on remote sensing techniques using airborne or space borne sensors. These calibration activities are performed to account for the characterisation errors or undetermined post-launch changes in sensor performance. We had measured the surface reflectance and atmospheric variables at the site synchronising with HySIS sensor overhead pass. Top of the atmosphere (TOA) spectral radiances are computed using 6SV2.1 (Second Simulation of the Satellite Signal in the solar Spectrum) radiative transfer (RT) code with the surface reflectance and atmospheric variables as well as spectral response function (SRF) of individual channel. The results of in-orbit radiometric calibration of the HySIS hyperspectral imager along with the uncertainties in computed calibration coefficients due to various parameters are described in this report. Results show that the preflight calibrations of HySIS are probably not consistent with in-flight performance of the instrument. The V4 (fourth version) data sets of HySIS sensor improves the agreement to the vicarious calibration exercise prediction.</p>
10.Key Words	Calibration, reflectance, aerosol, radiative transfer, uncertainty
11.Security classification	Unrestricted
12.Distribution statement	Within centre

1. Table of contents

2. Abstract.....	4
3. Introduction	5
4. Data and Methodology	6
5. HySIS Radiance Calculation	7
6. Calibration site and field measurements.....	7
Field Campaign.....	9
Atmospheric Measurements.....	9
Surface Reflectance	10
7. Methodology.....	11
Statistical analyses	13
8. Results and Discussion	14
9. Conclusion.....	20
10. Acknowledgement	21
11. References.....	21

2. Abstract

The absolute radiometric calibration of a satellite sensor is the critical factor that ensures the usefulness of the acquired data for quantitative applications on remote sensing techniques using airborne or space borne sensors. These calibration activities are performed to account for the characterisation errors or undetermined post-launch changes in sensor performance. We had measured the surface reflectance and atmospheric variables at the site synchronising with HySIS sensor overhead pass. Top of the atmosphere (TOA) spectral radiances are computed using 6SV2.1 (Second Simulation of the Satellite Signal in the solar Spectrum) radiative transfer (RT) code with the surface reflectance and atmospheric variables as well as spectral response function (SRF) of individual channel. The results of in-orbit radiometric calibration of the HySIS hyperspectral imager along with the uncertainties in computed calibration coefficients due to various parameters are described in this report. Results show that the preflight calibrations of HySIS are probably not consistent with in-flight performance of the instrument. The V4 (fourth version) data sets of HySIS sensor improves the agreement to the vicarious calibration exercise prediction.

3. Introduction

The quantitative analysis of images produced by satellite-borne radiometers requires knowledge of their calibration, since the applications of modern satellite data requires higher quantitative accuracy and validity. Monitoring the radiometric characteristics of satellite sensors is an essential step in the estimation of reliable, continuous variables for the quantitative applications. This radiometric calibration, which converts the electronic digital number (DN) to physical units, has been performed to acquire consistently accurate radiometric information over a specifically designed sensor's life-time (Belward, 1999, Liang, 2004). To secure radiometric calibration and the continuity of satellite data from multiple sensors, pre- and post-launch calibration has been proposed to determine the characteristics of radiometric calibration (Butler and Barnes, 1998, Chen, 1997, Dinguirard and P. N. Slater, 1999). The pre-calibration step, which is conducted in a controlled laboratory setting, uses a well-characterized radiant source. However, because calibrated sensors are degraded by the severe environmental conditions encountered after launch (Hagolle, et. al., 1999), operational space-borne satellites need to be monitored for their absolute radiometric characteristics while in orbit. For in-flight calibration of satellites, on-board, vicarious, lunar, and cross-calibration techniques have been suggested for radiometric calibration (Abdou, et. al., 2002, Kerola, et. al., 2009, Kamei, et. al., 2012, Liu, et. al., 2010, Seo, 2014, Thome, et. al., 2003) apart from pre-launch laboratory calibration. On-board calibration is performed in orbiting satellites using well-known sources such as artificial lamps or the sun. On-board calibrators have the advantage of allowing frequent response determinations. However, they increase the cost and weight of instruments. Vicarious and cross-calibration techniques are used for systems without on-board calibrators. These techniques also act as a validation tool for systems with on-board calibrators (Kamei, et. al., 2012, Liu, et. al., 2010, Pagnutti, et. al., 2003).

Absolute in-orbit calibration can be done in two ways: (1) with an on-board calibration sources, i.e., known light sources, solar radiation, or (2) by vicarious calibration where a portion of the earth viewed by the instrument becomes a calibration source. The method of vicarious calibration by means of calculated radiance allows absolute calibration of satellite radiometers in orbit. It works by comparing either counts or engineering unit from the radiometer to be calibrated or reiterated with corresponding absolute radiances, calculated from actual values of relevant optically acting parameters of the atmosphere and the earth's surface. This vicarious

calibration, calculated radiances can be applied in every spectral region where the radiative transfer equation can be solved and the actual parameters are known.

The India's Hyper Spectral Imaging Satellite (HySIS) was successfully launched on 29th November 2018 in PSVL-C43 mission from Satish Dhawan Space Centre SHAR, Sriharikota. The primary goal of HySIS sensor is to study the Earth's surface in the visible, near infrared and shortwave infrared regions of the electromagnetic spectrum. This earth observing imaging spectrometer will operate in the 0.4 to 0.95 μm spectral range with 60 spectral bands having ~10nm spectral bandwidth and 0.885 to 2.473 μm spectral range with 256 spectral bands having ~5nm spectral bandwidth from an approximate 630km orbit. This scientific report brings the initial vicarious calibration results of HySIS sensor during its intense validation phase of the mission.

4. **Data and Methodology**

The desired absolute inflight calibration is achieved through repeated comparison of different counts with their corresponding radiances and hence the calibration value. For a specific count, as measured by the radiometer, all corresponding optically active parameters of the atmosphere and the underlying surface are determined. Based on these measurement, the absolute radiance L_t leaving the top-of-the-atmosphere and measured by the satellite is calculated. For a specific wavelength detector with linear response, the calibration values lie on a straight line and slope of the line is the calibration constant (c) or calibration gain coefficient (factor applied for data product generation from the calibrated sensor radiance).

$$L_t = c \cdot \text{count}$$

The radiation L_t consists of photons originating from the sun and scattered in the atmosphere or reflected at the surface. So the spectral radiance $L_{t\lambda}$ depend on the angles among sun, target and satellite, on the spectral extraterrestrial solar irradiance (corrected for sun, earth variation during the year) and on the spectral optical properties of atmosphere and surface.

In cloudless atmospheres, the relevant optical parameters are the turbidity, the scattering phase function and the single-scattering albedo, the absorption coefficient for absorption due to atmospheric gases, and the reflectance of the surface. If all these parameters are known or measured, the radiance to be measured by the satellite-borne radiometer can be calculated by

solving the radiative transfer equation. In practice, the method starts with a search for conditions where knowledge of the optical parameters is best or most simply achieved, because it makes calculation and data capture easier. The cloud free atmosphere further eliminates microphysical parameters of clouds which are difficult to measure.

Eventually, field campaigns are conducted over desert site in Little Rann of Kutch (LROK) to obtain hyperspectral surface reflectances using handheld radiometric instruments. Several important environmental conditions are necessary, such as characterizations without cloud cover and a flat homogeneous surface to derive very consistent calibration coefficients. Other input parameters are also collected for the radiative transfer model simulation (e.g., atmospheric constituents, such as aerosol optical depth, ozone column, and water vapour content) using well calibrated MicroTOPS-II sunphotometer and ozonemonitor during the field campaigns. The vicarious calibration methodology using Second Simulation of the Satellite Signal in the Solar Spectrum Vector Version (6SV2.1) radiative transfer simulations, based on measured atmospheric parameters, is effective for practical, rapid and low-cost radiometric calibration.

5. HySIS Radiance Calculation

HySIS measured brightness values received in terms of a digital number (DN) for each band are converted to TOA spectral radiance $L(\lambda)$ values using the calibration coefficients with zero dark count.

$$L = \left(\frac{L_{max} - L_{min}}{DN_{max}} \right) DN + L_{min}$$

Where $DN_{max} = 4095$, L_{max} is the saturation radiance derived from laboratory calibration exercise, L_{min} is the dark count.

6. Calibration site and field measurements

Attributing to their preferable stability of surface characteristics and atmospheric dynamics, pseudo invariant sites are commonly used for sensor radiometric calibration, degradation monitoring and inter-comparisons (Chander, et. al., 2010, Bouvet, 2014) especially for the satellite sensors without on-board calibration facilities. The Committee on Earth

Observation Satellites (CEOS) Working group on Calibration and Validation identified several test sites around the world (Teillet, et. al., 2010) based on the selection criteria, such as low probability of atmospheric variability, high spatial homogeneity, weak directional effects, flat reflectivity spectrum. Calibration sites are never chosen randomly, and to be adequate they must satisfy a certain number of criteria (Scott, et. al., 1996, Slater, et. al., 1996, Slater, et. al., 1987, Teillet, et. al., 1997). Based on these criteria, we have selected desert site Little Rann of Kutch (LRK) in Gujarat, India (Figure 1).

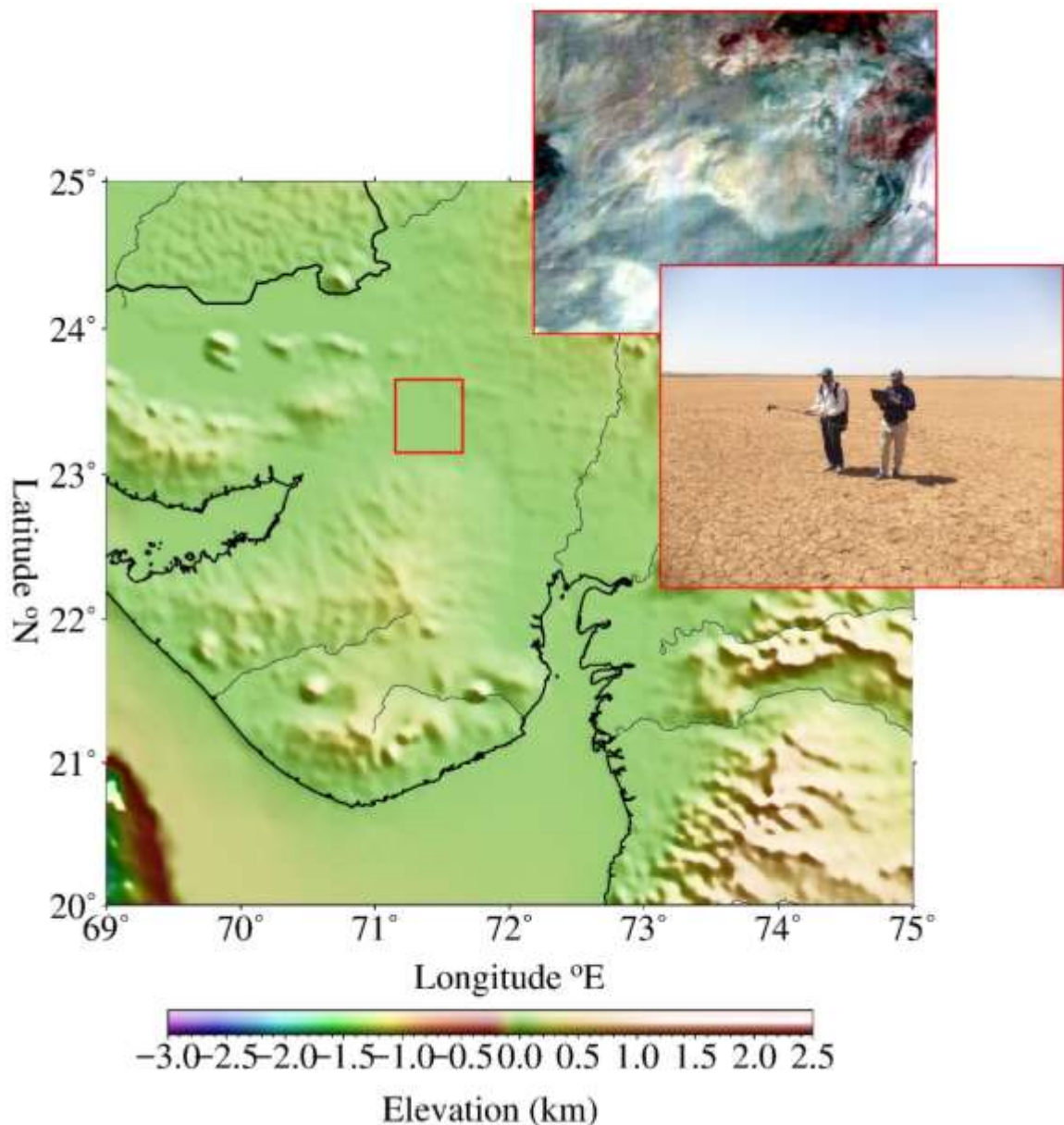


Figure 1: HySIS calibration campaign in Little Rann of Kuchchh

This site is a complete deserted site in Little Rann of Kutch (LRK), Gujarat with an altitude of ~6 m above mean sea level. This site is extended more than 60 km² area, presenting a

completely flat and homogenous terrain characterized by high surface reflectance. The area is a vast, homogenous, plain land with mostly dry, salty soil dominating the landscape during the months of December to May, and prone to excessive water logging during the monsoon season (June – September). The site is a clay-dominated dry land with different spectral characteristics that have been used for radiometric calibration including very large footprint sensors (e.g. INSAT-3A, INSAT-3D and INSAT-3DR).

Field Campaign

We performed field campaigns for vicarious calibration of HySIS at LRK test sites during 3rd February 2019. Simultaneous observations from satellite and ground have been successfully conducted, on ground the data sets are collected between 04:00 UTC and 07:00 UTC to cover maximum possible satellite overpass with the suitable atmospheric conditions.

Atmospheric Measurements

Since the algorithm employed radiative transfer calculations in the atmosphere, the specification of atmospheric conditions is necessary including the thermodynamic condition. However, we have measured aerosol optical depth (AOD), total columnar ozone (TCO) and total water vapour content (WVC) during field campaign. AOD measurements are carried out using a multi wavelength MicroTops-II sun-photometer (M/s. Solar Light Co., USA) at five different wavelengths at 380, 440, 500, 675 and 870 nm, from the solar instantaneous flux measurements with its internal calibration using the Langley method (Reagan, et. al.,1986, Schmid, et. al., 1995). The Full Width at Half Maximum (FWHM) bandwidth for the 380 nm channel is 2.4 ± 0.4 nm and 10 ± 1.5 nm for the other channels (Morys, et. al., 2001).

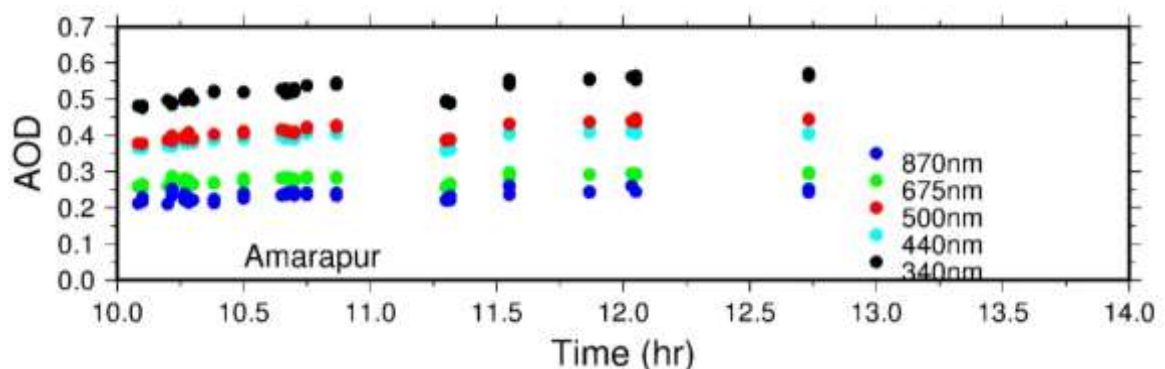


Figure 2: Variation of measured aerosol optical depth during the campaign.

A MicroTops-II Ozonometer, a ground-based instrument, which is capable of measuring the column ozone (CO) using three UV channels (305.5, 312.5, 320.0 nm) and the total water vapour content (WVC) using two near-IR channels (940 and 1020 nm) (Porter, et. al., 2001) as well as AOD at 1020 nm is also used during the field campaigns. More details of design, performance, error and calibration of MicroTops-II is given elsewhere (Morys, et. al., 2001, Porter, et. al., 2001). Figures 2 and 3 shows the variation of measured aerosol optical depth and column integrated values of watervapor and Ozone. The day of field campaign was prevailing with clear atmosphere with AOD at 870nm close to 0.2, atmospheric watervapor to 0.8 (dry atmosphere) and ozone was close to climatological mean value.

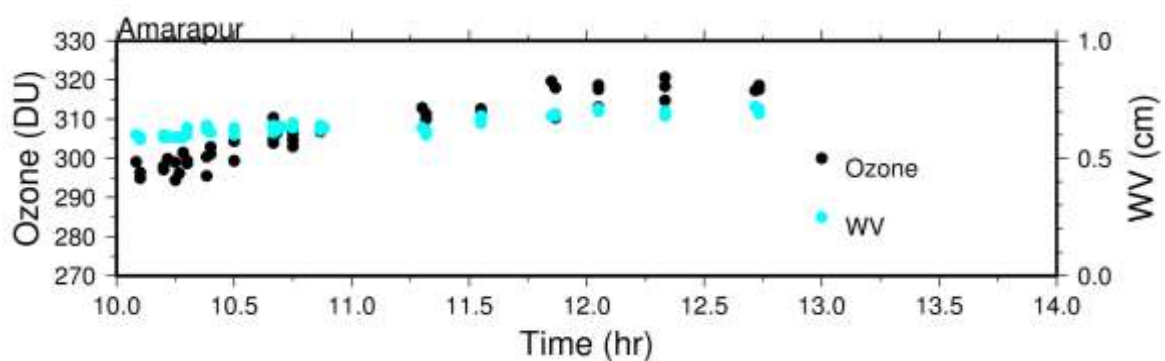


Figure 3: Variation of measured column integrated watervapor and Ozone during the campaign.

Surface Reflectance

Measurements of ground reflectance are carried out using a portable hyperspectral radiometer (FieldSpec-4 of M/s. Analytical Spectral Devices (ASD), Inc., 350-2500 nm). The fore-optic for light collection is projected out using a camera monopod to avoid the measurement noise, thereby ensuring that the surface being measured and free from shadows. The main unit is carried in a backpack, and the computer is carried on platform in front of the user. The reference measurements using Spectralon white plate are made at predetermined interval throughout the site collection. The ASD FieldSpec 4 has a 3-nm spectral resolution covering 350–1000 nm and a 10-nm spectral resolution in the 1000–2500 nm spectral range. To consider changeable light field conditions, optimization adjustments, dark correction, and white reference scan are conducted to obtain reliable target reflectance. All of the surface reflectance measurements are carefully processed. Figure 4 shows the mean measured surface reflectance along with standard deviation (at 1σ level). There are two peaks in the reflectance curve. The first gap around 1380nm is due to water vapour absorption. The second gas near

1800nm is due to a combination of high atmospheric absorption and low SNR in the field spectrometer where there is a change in detector and grating.

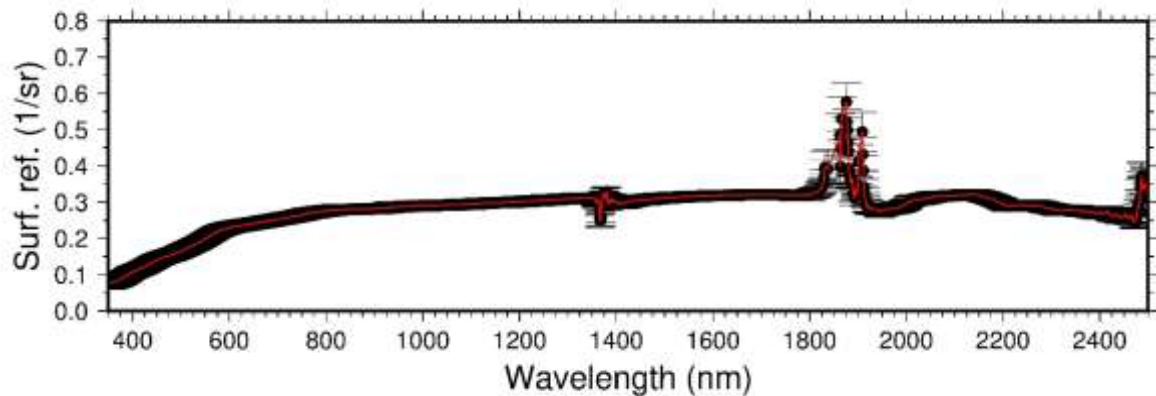


Figure 4: Mean surface reflectance along with standard deviation (1σ level).

7. Methodology

Reflectance-based and radiance-based techniques are the most common approaches when in-situ data are used to calibrate satellite sensors (Slater, et. al., 1987). Reflectance-based technique is used in this study, because it is difficult to maintain the radiometric accuracy of the spectrometer that measures the surface radiance in the radiance-based technique. The reflectance-based technique mainly depends on the measured ground surface reflectance and the incident solar irradiance on the surface under measurements. The reflectance is characterized by the ratio of measurement of the site to those of a standard reflectance/ Spectralon panel for which the bidirectional reflectance factor is precisely determined. The vicarious radiometric calibration depends on the surface reflectance and radiance from the sun to earth's surface and earth's surface to sensor and atmospheric optical thickness over the calibration site at the time of satellite pass. The ground measurements are used as an inputs for radiative transfer (RT) code for the simulation of absolute radiances in the required bands at the sensor level. The ground measurements are used to define the spectral directional reflectance of the surface and the spectral optical depth that are used to describe the aerosol and molecular scattering effect in the atmosphere (Gellman, et. al., 1991) along with this we used columnar water vapour to include the water vapour absorption effect along the path length of surface to satellite sensor. We have used improved 6SV2.1 RT code (here after 6SV) (Kotchenova, et. al., 2008, Vermote, et. al., 2006) to compute the radiance field using ground measurements which is very well calibrated, widely used and well documented radiative

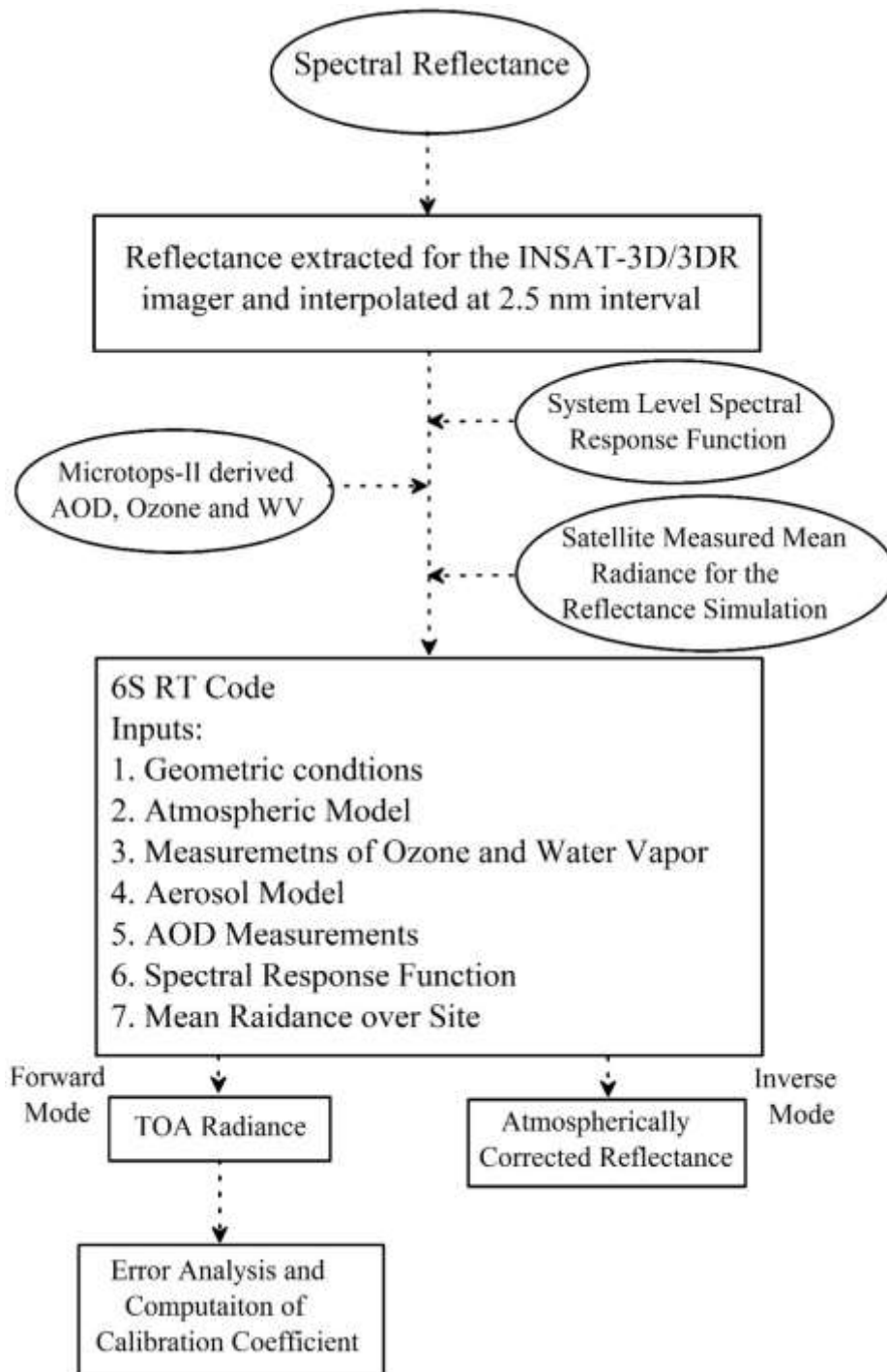


Figure 5: Flow chart of TOA spectral radiance simulation and estimation of calibration coefficient.

transfer model. The version 2.1 predicts the radiation arising from polarization effect of molecular and aerosol particles. 6SV RT model is a physically based model, which is not specified for particular satellite or test sites. In addition, 6SV RT model has spectral libraries for gaseous absorption and scattering by aerosols and molecules. 6SV deals better with atmospheric scattering than other RT models (Markham et al., 1992). 6SV model was

formulated for the atmospheric correction in the short wavelengths. 6SV code requires the geometric conditions, including the viewing zenith, viewing azimuth, solar zenith and solar azimuth angles. Viewing zenith and viewing azimuth angles are obtained from satellite metadata files and solar zenith and solar azimuth angles are calculated using time and location for a given data point.

Figure 5 describes with flow diagram for the simulation of TOA spectral radiance and estimation of calibration coefficient. For the RT simulation to derive the vicarious calibration coefficient the optimum selection of aerosol type is important. The actual aerosol characteristics are often differing from standard aerosol models in the RT codes. It is difficult to precisely estimate the aerosol characteristics in the field campaign. This leads to the systematic errors in the calibration results (Chen, et. al., 2014). However, in the present study we have used handheld MicroTops-II sunphotometer for the measurements of AOD. This cannot provide other optical and physical properties of aerosols (e.g. volume size distribution, refractive indices etc.), which helps to improvise the aerosol parameterization in the RT model and leads to high accuracy of TOA spectral radiance simulation.

Additionally, to reflect the characteristics of HySIS spectral bands, the normalized spectral response function (SRF)s are also used as inputs in the 6SV RT model to simulate the TOA spectral radiance. Both the SRF and measured surface reflectance data are resampled to 2.5 nm intervals using a spline interpolation method. The 6SV RT model computes TOA spectral radiance in the forward mode, while it computes atmospherically corrected surface reflectance in the inverse mode. 6SV RT model provides an output in the form of TOA spectral radiance, which is divided by the corresponding radiance observed by the HySIS for particular channel to yield calibration coefficients.

Statistical analyses

Statistical analyses are carried out for the additional information on how accurately the satellite measurement agrees with simulated values using in-situ measurements. Thus, the Root Mean Square Error (RMSE) to characterize the bias of algorithms in absolute terms is computed using Eq. (3):

$$RMSE = \frac{\sqrt{\frac{1}{n} \sum_1^n (estimated - measured)^2}}{\frac{1}{n} \sum_1^n (measured)} \quad (3)$$

The percentage of uncertainty is calculated using the following equation (4):

$$Percentage\ of\ uncertainty = \frac{(Uncertainty)}{Value} \times 100 \quad (4)$$

$$Uncertainty = \sqrt{\frac{Stdev}{(N - 1)}}$$

8. Results and Discussion

Total 55 surface spectral measurements were carried out on 3rd February 2019 over Amrapur site of Little Rann of Kuchchh synchronous to the HySIS satellite pass. Random surface measurements were done using ASD Field Spec. radiometer of fourth generation and the geo-locations are shown in Figure 6. The site used is fairly large and homogeneous to minimize the

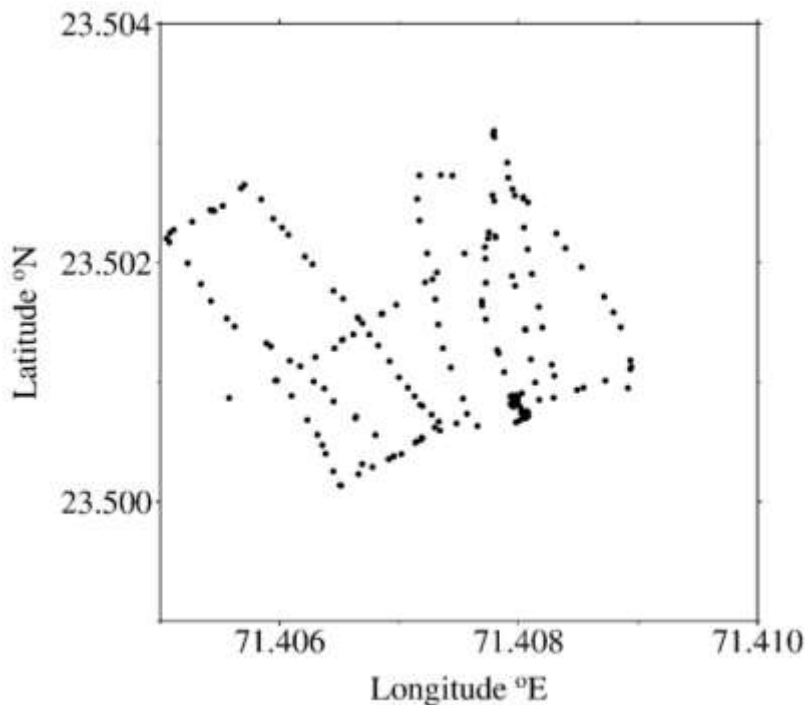


Figure 6: the geo-location of random surface reflectance measurements over Little Rann of Kuchchh on 3rd March 2019.

effects of surface nonuniformity and the adjacency effect. The in-situ measurements are used to determine the spectral directional reflectance of the surface and the spectral optical depth

components causing scattering in the atmosphere. These data are used as inputs to a radiative transfer code which computes the radiance field at an angular grid at various heights in the atmosphere. The code also computes the effect of ozone absorption based on a nominal vertical profile and an estimate of the total column ozone amount derived from the optical depth measurement. However, due to lack of other measurements the aerosol model selection is optimized by running the mean surface hyper-spectral reflectance against 6 standard aerosol models (Urban, continental, desert, marine, biomass burning, and stratosphere) defined in the radiative transfer model. We found a closer agreement with Urban aerosol model solution as compared to the other aerosol model selections and hence it was chosen to perform the TOA simulations for every surface measurement carried over various geo-locations as depicted in Figure 6. The model simulation was done at 2.5nm spectral sampling interval using the HySIS spectral response function derived during the lab calibration exercises. Band average radiance is computed given the spectral response of each sensor spectral band for the final comparison and the results are shown in Figure 7 for the VNIR bands and Figure 8 for the SWIR bands.

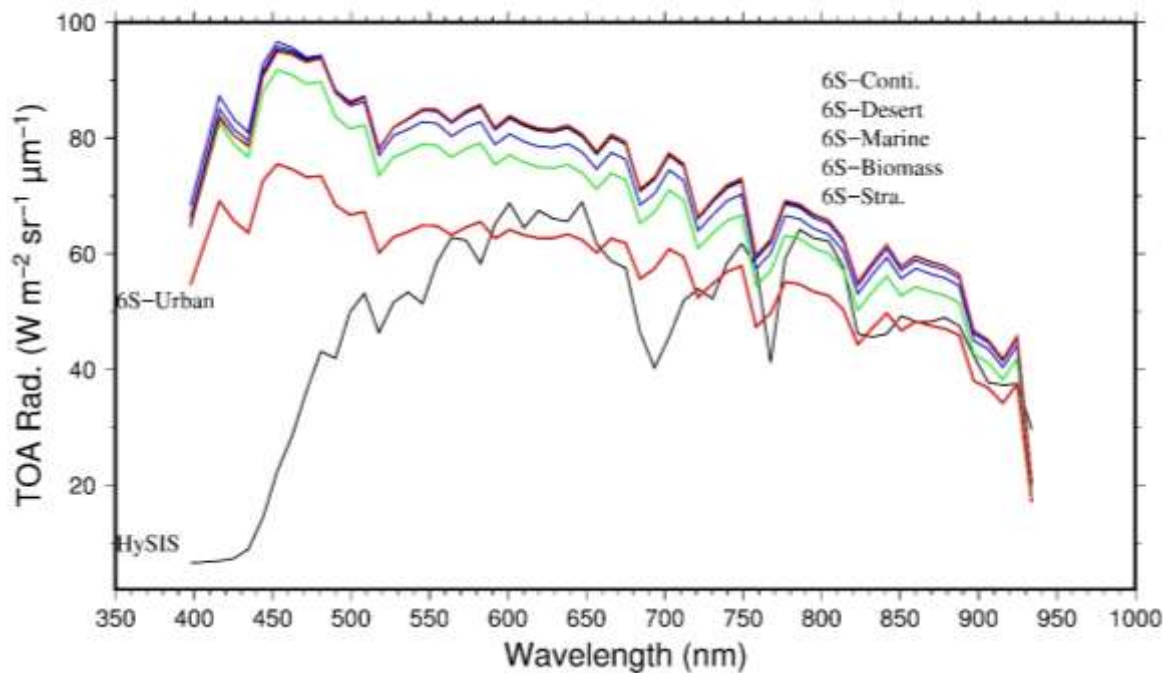


Figure 7: HySIS VNIR bands performance against 6S simulation for various aerosol models.

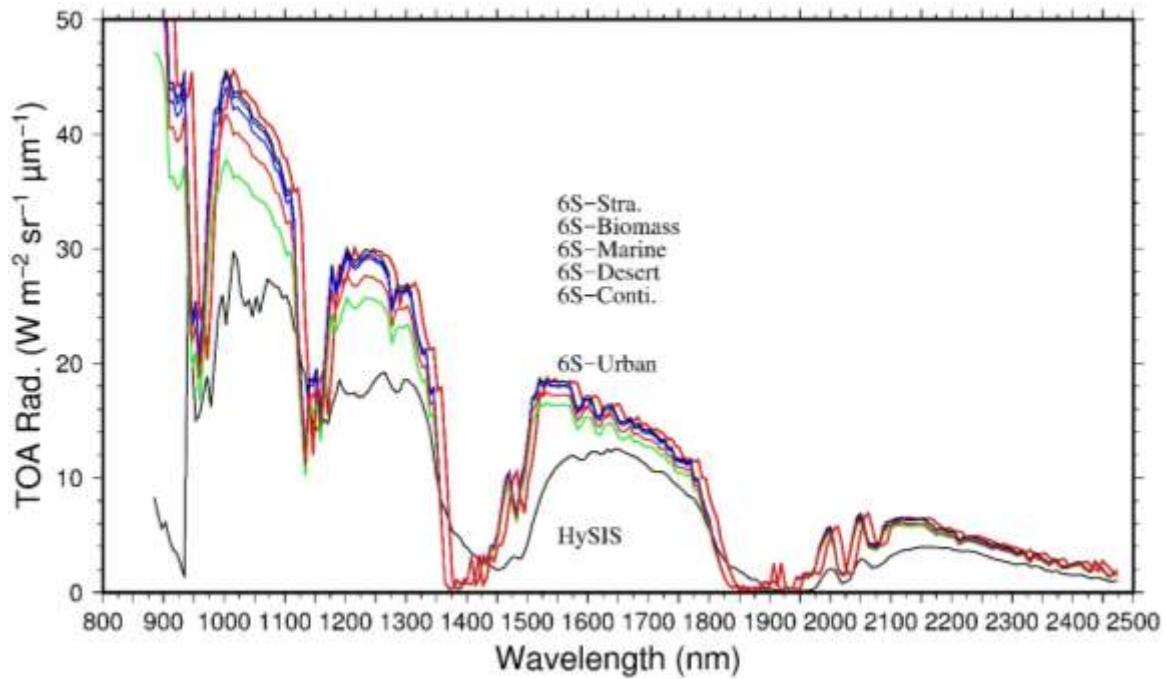


Figure 8: HySIS SWIR bands performance against 6S simulation for various aerosol models.

The figure 9 and 10 shows HySIS sensor measured TOA radiance averaged over 5x5 pixels centred over the measurement campaign (solid red line) and 6S model performance. The solid blue line shows the spectral mean values of 55 model simulation with respect to measured individual surface reflectance and the standard deviation is shown as error bars. The presence of uncertainty is shown in down panel. Since the instrument measured reflectance centred around water vapour absorption regions (1380nm) and a combination of high atmospheric absorption and low SNR in the field spectrometer where there is a change in detector and grating are invalid (around 1800nm), the model simulation and its comparison around these spectral window is avoided, for the purpose of completing graph plots Figures 9 and 10 are shown here without any gaps. Figure 11 shows the comparison for the full spectral range of HySIS sensor.

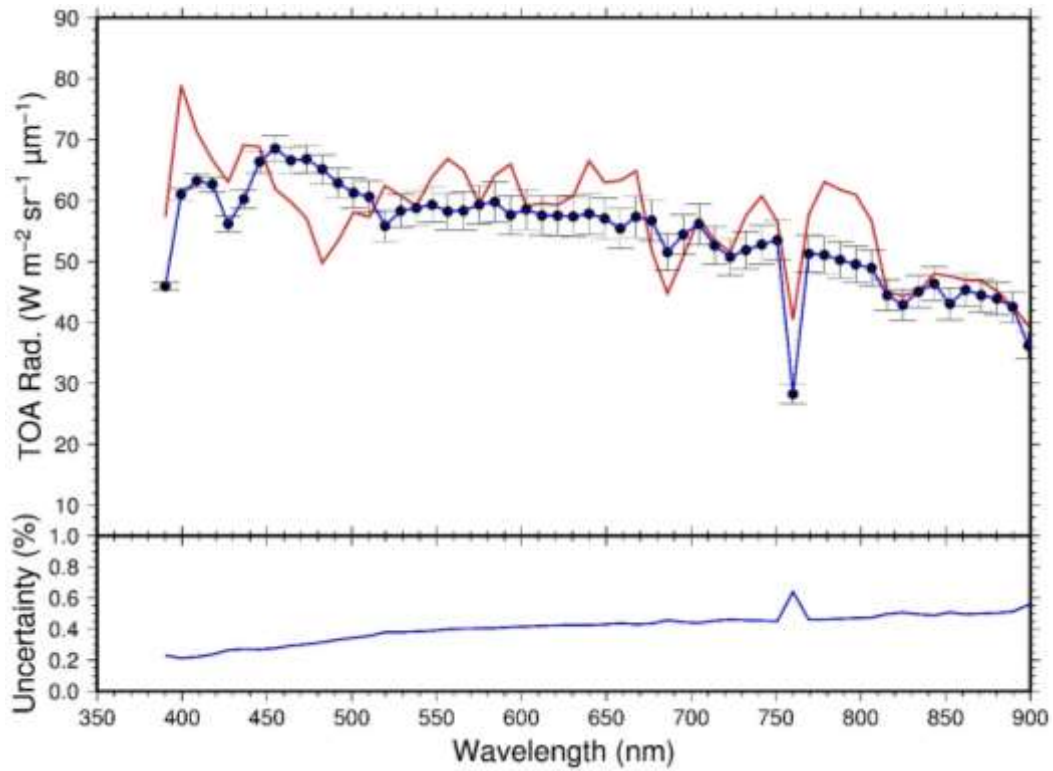


Figure 9: HySIS VNIR bands performance (solid red line) against 6S simulation for Urban aerosol model solution (solid blue line).

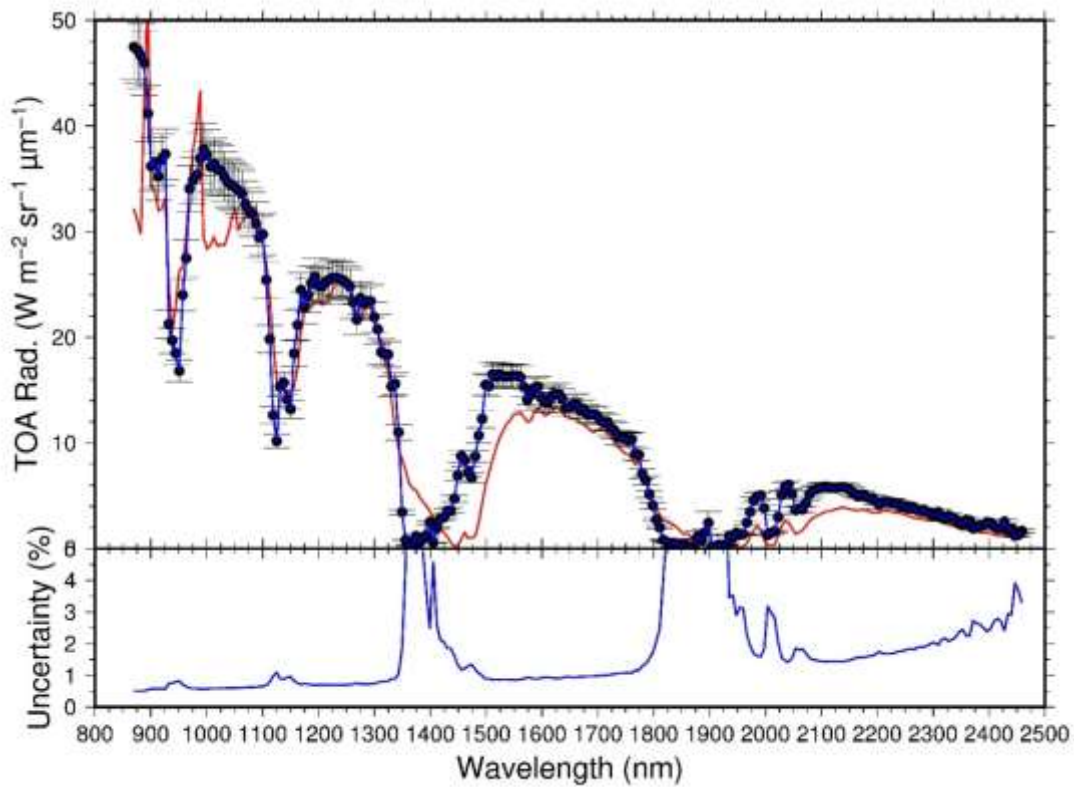


Figure 10: HySIS SWIR bands performance (solid red line) against 6S simulation for Urban aerosol model solution (solid blue line).

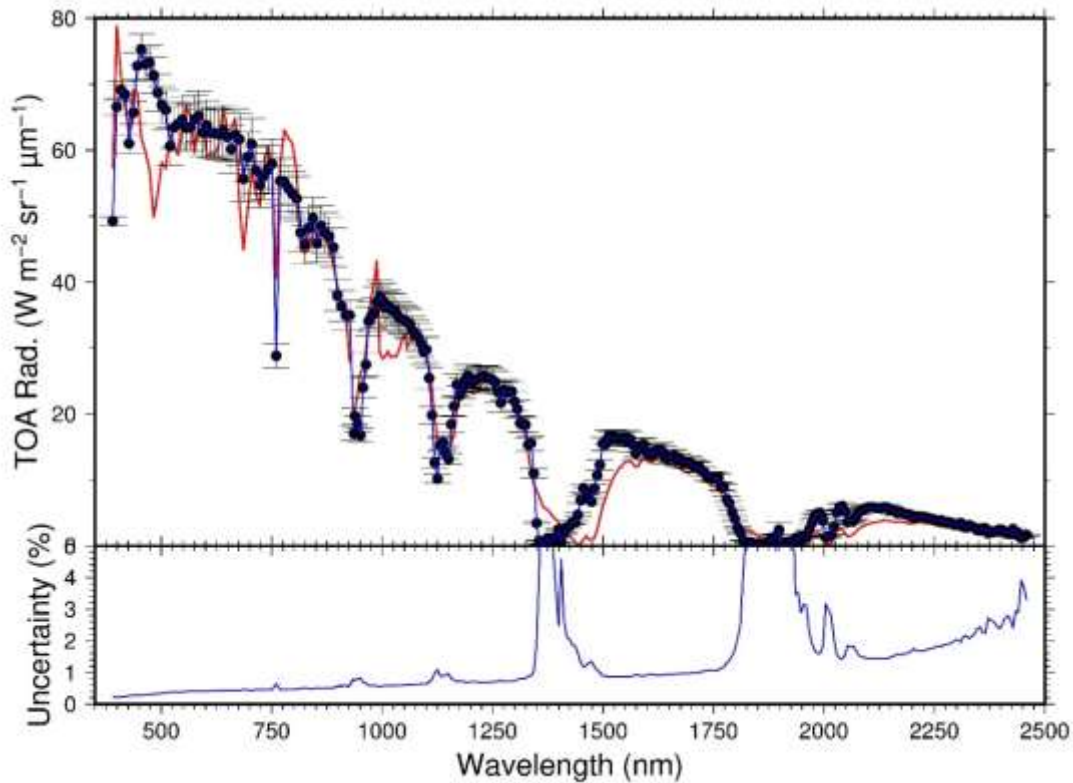


Figure 11: HySIS bands performance (solid red line) against 6S simulation for Urban aerosol model solution (solid blue line).

Figure 12 shows the scatter plot of top-of-the-atmosphere are observed by HySIS sensor and 6S model simulation. Here the mean values are plotted respectively for VNIR and SWIR spectral region. The observed root mean square error of HySIS sensor for the VNIR region is $6.71 \text{ W/m}^2/\text{sr}/\mu\text{m}$ which is $\sim 9.5\%$ of radiance observed at 500nm spectral region. The observed difference may be due to slight over estimation of HySIS sensor. However, it is statistically invalid to conclude such results with single date campaign. The calibration team strongly relies on multi-date measurement campaign for the conclusion. The performance of SWIR region is similar as compare to VNIR with better correlation coefficient (0.93), which means the spectral absorption characteristics of atmosphere and sun is well captured by the sensor.

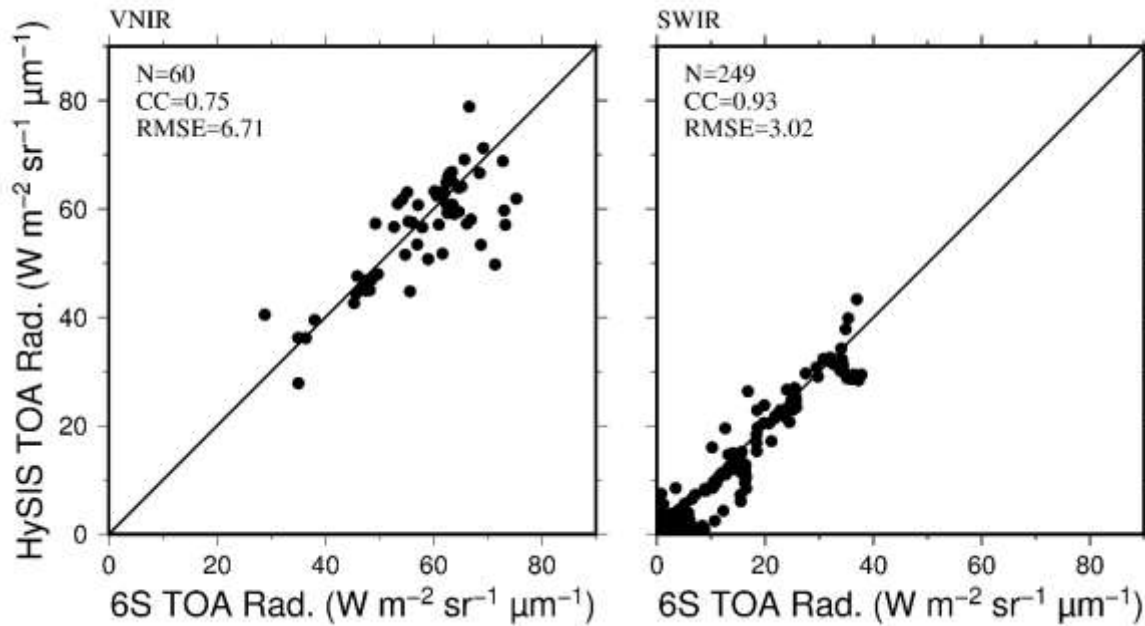


Figure 12: Scatter plot of mean HySIS and mean 6S simulated TOA radiance for VNIR and SWIR spectral region.

Uncertainty in the calibration results from uncertainty in the measurement and calculated radiances. The more accurate these quantities are and the more calibration values are used to determine the calibration curve, the less is its uncertainty. Of course, different parts of the image or different times are used to derive the calibration curve, the response of the radiometer is assumed to be stable over the image for the duration of the calibration. On the other hand, multiple calibration at different times allows a check on whether the radiometer is drifting. The uncertainty in the calculated radiances results from uncertainty of the optical parameters used and from imprecision of the calculation procedure. Such an improvement is simplest for radiometers which respond linearly to the incoming radiation. Then the result of the calibration procedure is one calibration constant, the slope of the straight line determined from the calibration values. The divergence of the calibration values from the line gives a check on their validity and so on the validity of the optical data taken from the atmosphere and the reflectance. Statistical uncertainties of the data result in a lower regression coefficient but not in uncertainty in the calibration constant. However, systematic errors would change the slope of the straight line and so give an error in the calibration constant.

Table 1: The error budget in vicarious calibration HySIS sensor using 6SV2.1 and field measurements.

Source of Uncertainty	Percentage of uncertainty
Aerosol optical depth	5.99
Integrated water vapour	3.71
Integrated Ozone	0.12
6S model	~3 (maximum)
Surface reflectance measurements	
Spectralon panel calibration	0.3
Ground measurement errors	17
Inherent code accuracy	0.6
Total uncertainty (root sum of squares)	18

Table 1 shows the detailed error budget in doing the vicarious calibration of HySIS sensors using 6SV2.1 radiative transfer model and field measurements carried out on 3rd February 2019 at Little Rann of Kuchchh site. The total uncertainty is ~18% and major error source is the surface reflectance condition (~17%). As the image was acquired around 10:30am when the surface solar irradiance changes quite fast with time and also the site is not much dry where usually large amount of surface cracks used to present. These surface manifestation makes surface near Lambertian surface and thus spatial uniformity used to present.

9. Conclusion

The absolute radiometric calibration of a satellite sensor is the critical factor that ensures the usefulness of the acquired data for quantitative applications on remote sensing techniques using airborne or space borne sensors. Calibration also allows for a correction of instrument drift over time and for comparison of datasets from different sensors. Accurate radiometric calibration of a sensor allows for atmospheric correction of data and retrieval of surface reflectance. We had measured the surface reflectance and atmospheric variables at the site synchronising with HySIS sensor overhead pass on 3rd February 2019. Top of the atmosphere (TOA) spectral radiances are computed using 6SV2.1 (Second Simulation of the Satellite Signal in the solar Spectrum) radiative transfer (RT) code with the surface reflectance and atmospheric variables as well as spectral response function (SRF) of individual channel. Results show that the preflight calibrations of HySIS are probably not consistent with in-flight performance of the instrument. The V4 (fourth version) data sets of HySIS sensor improves the agreement to the vicarious calibration exercise prediction.

The results of V4 data sets are:

The observed root mean square error of HySIS sensor for the VNIR region is $6.71 \text{ W/m}^2/\text{sr}/\mu\text{m}$ which is $\sim 9.5\%$ of radiance observed at 500nm spectral region. The observed difference may be due to slight over estimation of HySIS sensor.

The performance of SWIR region is similar as compare to VNIR with better correlation coefficient (0.93), which means the spectral absorption characteristics are well captured by the sensor measurements.

The total uncertainty is $\sim 18\%$ and major error source is the surface reflectance condition ($\sim 17\%$). As the image was acquired around 10:30am when the surface solar irradiance changes quite fast with time and also the site is not much dry where usually large amount of surface cracks used to present. These surface manifestation makes surface near Lambertian surface and thus spatial uniformity used to present.

However, it is statistically invalid to conclude such results with single date campaign. The calibration team strongly relies on multi-date measurement campaign for the conclusion.

10. Acknowledgement

The authors gratefully acknowledge the encouragement received from Director, SAC for carrying out the present research work. Valuable suggestions received from Deputy Director, EPSA are also gratefully acknowledged. Authors are thankful to Dr. Mehul and SIPG data product team and Cal-Val team members for their supports.

11. References

Belward, S., International co-operation in satellite sensor calibration; the role of the GEOS working group on calibration and validation, 1999. *Adv. Space Res.*, vol. 23, no. 8, pp. 1443–1448.

Liang, S., *Quantitative Remote Sensing of Land Surface*. New York, NY, USA: Wiley, 2004, pp. 178–194.

Butler, J. J. and Barnes, R. A., Calibration strategy for the Earth Observing System (EOS)-AM1 platform, 1998. *IEEE Trans. Geosci. Remote Sens.*, vol. 36, no. 4, pp. 1056–1061.

Chen, H. S., *Remote Sensing Calibration Systems: An Introduction*. Hampton, VA, USA: Deepak, 1997.

- Dinguirard, M., and Slater, P. N., Calibration of space-multispectral imaging sensors: A review, 1999. *Remote Sens. Environ.*, vol. 68, no. 3, pp. 194–205.
- Hagolle, O., et al., Results of POLDER in-flight calibration, 1999. *IEEE Trans. Geosci. Remote Sens.*, vol. 37, no. 3, pp. 1550–1566.
- Abdou, et. al., W. A., Vicarious calibration experiment in support of the multi-angle imaging spectroradiometer, 2002. *IEEE Trans. Geosci. Remote Sens.*, vol. 40, no. 7, pp. 1500–1511.
- Kerola, D. X., Bruegge, C. J., Gross, H. N., and Helmlinger, M. C., Onorbit calibration of the EO-1 Hyperion and Advanced Land Imager (ALI) sensors using the LED Spectrometer (LSpec) automated facility, 1999. *IEEE Trans. Geosci. Remote Sens.*, vol. 47, no. 4, pp. 1244–1255.
- Kamei, A., et al., Cross calibration of FORMOSAT-2 Remote Sensing Instrument (RSI) using Terra Advanced Spaceborne Thermal Emission and Reflectance Radiometer (ASTER), 2012. *IEEE Trans. Geosci. Remote Sens.*, vol. 50, no. 11, pp. 1–11.
- Liu. Et. al., C. C., Vicarious calibration of the FORMOSAT-2 remote sensing instrument, 2010. *IEEE Trans. Geosci. Remote Sens.*, vol. 48, no. 4, pp. 2162–2169.
- Seo, S. B. Relative compensation method for degradation of visible detectors using improved direct histogram specification, 2014. *Electron. Lett.*, vol. 50, no. 6, pp. 446–447.
- Thome, K. J., Bigger, S. F., and Wisniewski, W., Cross comparison of EO-1 sensors and other Earth resources sensors to Landsat-7 ETM+ using Railroad Valley Playa, 2003. *IEEE Trans. Geosci. Remote Sens.*, vol. 41, no. 6, pp. 1180–1188.
- Pagnutti, M., et. al., Radiometric characterization of IKONOS multispectral imagery, 2003. *Remote Sens. Environ.*, vol. 88, no. 1/2, pp. 53–68.
- Chander, G., Xiong, X., Choi, T., Angal, A., Monitoring on-orbit calibration stability of the Terra MODIS and Landsat 7 ETM_p sensors using pseudo-invariant test sites, 2010. *Remote Sens. Environ.* 114, 925–939.
- Bouvet, M., Radiometric comparison of multispectral imagers over a pseudo-invariant calibration site using a reference radiometric model, 2014. *Remote Sens. Environ.* 140, 141–154.
- Teillet, P., Chander, G., Terrestrial reference standard sites for post-launch sensor calibration, 2010. *Can. J. Remote Sens.* 36, 437–450.
- Scott, K. P., Thome, K. J., Brownlee, M., Evaluation of the railroad valley playa for use in vicarious calibration, 1996. *Proc. SPIE* 2818, 158–166.
- Slater, P. N., Biggar, S. F., Thome, K. J., Gellman, D. I., Spyak, P. R., Vicarious radiometric calibrations of EOS sensors, 1996. *J. Atmos. Ocean. Technol.* 13, 349–359.
- Slater, P. N., Biggar, S. F., Holm, R. A., Jackson, R. D., Mao, Y., Moran, M. S., Palmer, J. M., Yuan, B., Reflectance- and radiance-based methods for in-flight absolute calibration of multispectral sensors, 1987. *Remote Sens. Environ.* 22, 11–37.

- Teillet, P. M., Horler, D., O'Neill, N.T., Calibration, validation, and quality assurance in remote sensing: a new paradigm, 1997. *Can. J. Remote Sens.* 23 (4), 401–414.
- Reagan, J. A., Thomason, L.W., Herman, B. M., Palmer, J. M., Assessment of atmospheric limitations on the determination of the solar spectral constant from ground-based spectroradiometer measurements, 1986. *IEEE Trans. Geosci. Remote Sens.* GE-24, 258– 266.
- Schmid, B., Wehrli, C., 1995. Comparison of sun photometer calibration by use of the Langley technique and standard lamp. *Appl. Opt.* 34, 4500–4512.
- Morys, M., Mims III, F. M., Hagerup, S., Anderson, S. E., Baker, A., Kia, J., Walkup, T., 2001. Design, calibration, and performance of MICROTOPS II handheld ozone monitor and Sun photometer. *J. Geophys. Res.* 106 (D13), 14573–14582.
- Porter, J. N., Miller, M., Pietras, C., Motell, C., 2001. Ship-based Sun photometer measurements using microtops Sun photo-meters. *J. Atmos. Ocean. Technol.* 18, 765–774.
- Gellman, D. I., Biggar, S. F., Slater, P. N., Bruegge, C. J., 1991. Calibrated intercepts for solar radiometers used in remote sensor calibration. *Proc. SPIE* 1493, 19–24.
- Kotchenova, S.Y., Vermote, E. F., Levy, R., Lyapustin, A., 2008. Radiative transfer codes for atmospheric correction and aerosol retrieval: intercomparison study. *Appl. Opt.* 47 (13), 2215–2226.
- Vermote, E. D., Tanre, J. L., Deuze, M., Herman, J. J., Morcrette, Kotchenova, S.Y., 2006. *Second Simulation of Satellite Signal in the Satellite Spectrum (6S). 6S User Guide Version 3.* University of Maryland.
- Markham, B. L., Halthore, R. N., Goetz, S. J., 1992. Surface reflectance retrieval from satellite and aircraft sensors: results of sensor and algorithm comparison during FIFE. *J. Geophys. Res.* 97. (D17718), 7857795.
- Chen, Z., Zhang, B., Zhang, H., Zhang, W., 2014. Vicarious calibration of Beijing-1 multispectral imagers. *Remote Sens.* 6, 1432–1450, <http://dx.doi.org/10.3390/rs6021432>.